# Many-body effects and carrier dynamics in CdSe/CdS Stark superlattices

W. Langbein, M. Hetterich, and C. Klingshirn
*Institut für Angewandte Physik, Universität Karlsruhe, D-76128 Karlsruhe, Germany*
(Received 11 October 1994)

Strained CdSe/CdS superlattices show very strong intrinsic piezoelectric fields due to the high piezoelectric constants in combination with a large lattice mismatch of 3.9%. The linear as well as the nonlinear optical properties are formed by these fields, which dominate the band structure. We report on the excitation-density-dependent luminescence and absorption of these superlattices grown by hot-wall beam epitaxy and compare the experimental results with a theory including both the electrostatic screening and the band-gap renormalization.

## I. INTRODUCTION

The occurrence of piezoelectric fields in strained-layer superlattices consisting of materials without inversion symmetry along the growth axis leads to a substantial change of the electronic structure and of the linear and nonlinear optical properties.[1] They result in large nonlinear optical effects due to the screening of these fields by the charge of the carrier density. For superlattices consisting of III-V zinc-blende-type compounds such as $GaAs/Ga_xAs_{1-x}P$,[2] $In_xGa_{1-x}As/GaAs$,[3,4] $In_x\ Ga_{1-x}As/Al_y\ Ga_{1-y}As$,[5] and the II-VI $CdTe/Cd_xZn_{1-x}Te$,[6] these fields are in the order of $10^7$V/m and, consequently, the piezoelectric fields can often be treated as a perturbation of the original band structure. The corresponding energy shifts of the transition energies are in the order of a few ten meV. Higher piezoelectric fields are expected in various cubic and hexagonal II-VI compounds due to their large piezoelectric constants reflecting the more polar binding.

Recent progress in the growth of CdSe/CdS II-VI superlattices by hot-wall beam epitaxy[7–9] (HWBE) and metal organic chemical vapor deposition (MOCVD) has made it possible to investigate this material system, which exhibits very strong internal piezoelectric fields of about $10^8$V/m along the $\vec{c}$ axis of the hexagonal crystal structure, which represents also the growth direction.[10] This is due to the combination of II-VI materials with a large lattice mismatch of 3.9 %. The critical thickness for this system and this growth direction is relatively high as indicated by the fact that SL's with periods up to 10 nm show hardly any relaxation, as determined by the SL photoluminescence. This can be explained by the missing half-loop mechanism prominent for the strain relaxation in zinc-blende-type materials.[7,11] The band alignment of the CdSe/CdS system is type II with a conduction-band offset of about 150 meV (Refs. 10 and 12) (see Fig. 1). The piezoelectric fields lead to a redshift of the lowest transition energy of 180 meV per nm period length in a symmetric SL (see the discussion with Fig. 6 below), which broadens the luminescence considerably even in samples with an interface fluctuation of only one monolayer (0.56 nm).

The previous investigations by Halsall[13] on this system were performed on samples grown by MOCVD on GaAs substrate. They concentrate on the influence of the structural parameters on the optical transition energy of the superlattice. The band structure in the unexcited case is calculated[14] using a Kronig-Penney-like model. Time-resolved luminescence experiments with nanosecond time resolution show a redshift of the luminescence energy after high excitation,[15] which is significant for piezosuperlattices. Here, we report on picosecond high excitation time-resolved experiments and a theoretical model for the electronic states and transitions including the many-body effects band-gap renormalization (BGR) and charge-carrier screening. The paper is organized as follows: In Sec. II, we describe the samples and the experimental details, in Sec. III the time-resolved photoluminescence is discussed, in Sec. IV an analytical model for the observed logarithmic temporal shift of the lumi-

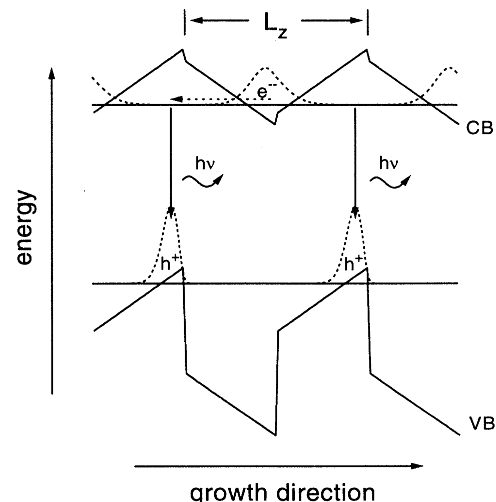


FIG. 1. Principal band structure and recombination process in the CdSe/CdS SL system. The conduction and valence-band edges (solid lines) are shown together with the squared envelope of the lowest (highest) conduction- (valence-) band state (dashed lines).

 ©1995 The American Physical Society

nescence peak energy is developed, in Sec. V the numerical model for the electronic states and transitions is presented and its results are compared with the experimental data, and in Sec. VI the nonlinear absorption in this system is discussed.

## II. SAMPLES AND EXPERIMENTAL SETUP

The samples used in our experiments were grown by HWBE on a GaAs ($\bar{1}\bar{1}\bar{1}$) B substrate.[7] They comprise a 4 $\mu$m CdS-buffer layer, which provides a strain-free wurtzite surface for the following superlattice, consisting of 30 periods of CdSe/CdS layers of nominal equal width and a 100 nm CdS cladding layer at the top of the structure (see Fig. 2). The three samples investigated in this paper have period lengths of 4 nm (sample I), 8 nm (sample II), and 12 nm (sample III), as determined by the positions of satellite peaks in high-resolution $\theta$ -2$\theta$ x-ray diffraction.

The principal band alignment in this SL system is depicted in Fig. 1. The discontinuities of the band gaps at the heterojunctions are obvious. The tilting of the band arises from the piezoelectric fields induced by the alternating strain in the layers.

The photoluminescence spectra of the samples at low excitation were measured at 4.2 K with an excitation power of about $10^{-3}$ W/cm$^2$, showing for the three above-mentioned samples broad luminescence bands centered around 1.67 eV, 1.42 eV, and 1.31 eV, respectively. Calculations of the transition energies with the above determined thicknesses match the experimental values without strain relaxation for samples I and II and with 30 % relaxation for sample III. This suggests a critical period length of about 10 nm in this SL system. This critical period length for a single layer implies that the SL relaxes relative to the buffer layer during the growth of the first some periods, depending on the period length, leading to a freestanding upper part of the SL. This assumption concerning the strain relaxation is not critical to the SL band structure since mobile charges would screen any average piezoelectric field present in a non-free-standing SL, leading to a very similar band structure except for the strain-induced band shifts, which are not important in this study.

The excitation source for the time-resolved experiments was an excimer-pumped quenched dye laser, which provides pulses of 70 ps duration at a photon energy of 2.46 eV with 100 $\mu$J pulse energy and a repetition rate of 10 Hz. The sample was cooled in an helium flow cryostat to a temperature of 5 K. The photoluminescence of the sample was dispersed by a 27 cm spectrometer and temporally resolved with a single shot streak camera. The readout system for the streak camera was a cooled charge-coupled device array. The probe beam for the nonlinear absorption experiments was a continuum from a dye-cell pumped by the excimer laser, emitting a 10 ns long and 100 nm broad band that determines the maximum detection range. These experiments were performed on a part of sample III with the GaAs substrate removed by selective etching.

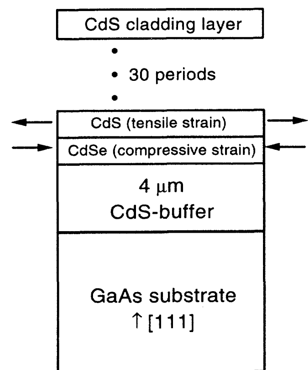


FIG. 2. Principal sample design of the HWBE-grown CdSe/CdS superlattices.

## III. PICOSECOND PHOTOLUMINESCENCE DYNAMICS

The time-resolved luminescence of sample II after high picosecond excitation of 0.3 mJ/cm$^2$, corresponding to a total created carrier density of about $10^{13}$/cm$^2$ per SL period, as calculated from the SL absorption, is shown in Fig. 3 on a logarithmic scale. At short times, the luminescence consists of two transitions, labeled ($e1$-$h1$) and ($e2$-$h1$). They correspond to the transition of electrons from the first (second) conduction subband to the first valence subband, respectively, as revealed by the comparison with a calculation (see Sec. V). The ($e2$-$h1$) transition is one order of magnitude stronger than the ($e1$-$h1$) transition, as is evident from the luminescence intensities. This finding is due to a stronger spatial overlap of the ($e2$) subband with the ($h1$) hole subband in comparison with the overlap of ($e1$) with ($h1$). Excitation with even higher intensities of $1-100$ mJ/cm$^2$ leads to stimulated emission

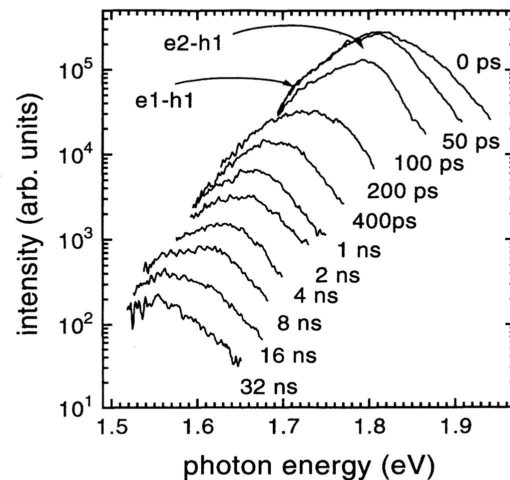


FIG. 3. Luminescence of sample III after excitation with 70 ps pulses at 2.46 eV, with 0.3 mJ/cm$^2$ for various times after excitation as indicated.

of the ($e2$-$h1$) transition, temporally following the excitation pulse.[16] With increasing time and thus decreasing carrier density, the ($e2$) subband is no longer occupied, and the luminescence of the ($e1$-$h1$) transition dominates and shifts with time to the red. This shift reveals a logarithmic time dependence (see Figs. 3 and 4) due to the temporal decrease of the charge-carrier screening introduced by the spatial separation of the electrons an holes in the type-II structure.

## IV. ANALYTICAL MODEL

To get a qualitative or even quantitative understanding of this logarithmic time development, which is established for times longer than the initial effective luminescence decay time of the ($e1$-$h1$) transition and shorter than times at which the carrier density becomes so low that it looses its influence on the band bending, one has to consider the temporal evolution of the overlap integral of the lowest subband states for conduction and valence band, e.g., $|\langle\psi_{e1}|\psi_{h1}\rangle|^2$, which determines the recombination rate together with the band-band matrix element of the zone-center Bloch-functions with the dipole operator. The latter value is nearly independent of the density and set constant in our calculation. A rough analytical estimation of the density dependent behavior of the overlap integral can be made using the formula for the transmission coefficient $T$ of a particle with energy $E_0$ through a triangular potential barrier $E(x)$ of the width $L_z/2$ for a symmetric SL with period $L_z$ (see Fig. 1):

$$T = \exp\left(-\frac{1}{\hbar}\int_0^{L_z/2}\sqrt{2m_e[V(z)-E_0]}dz\right). \qquad (1)$$

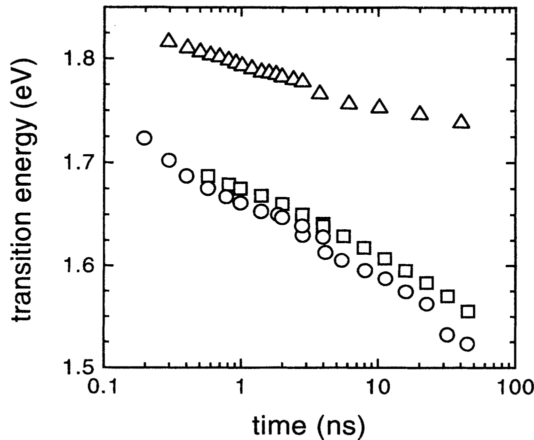


FIG. 4. Time development of the luminescence peak energies of sample I (triangles), sample II (squares), and sample III (circles) after picosecond excitation of $0.3\,\mathrm{mJ/cm^2}$ at 2.46 eV.

Only the tunneling of the electrons has to be considered due to the relative heavy hole masses in CdSe and CdS compared to the masses $m_e$ of the electrons. In our case the potential well for the electrons is given by the tilted CdS conduction band. We assume the screening of the piezoelectric field to be proportional to the carrier density in plane $\varrho$, which means neglecting the extent of the wave functions in the $z$ direction and get for the screened band tilting,

$$V(z) - E_0 = \frac{\varrho_0 - \varrho}{2\epsilon_0\epsilon}z, \qquad (2)$$

with the displacement charge $\varrho_0$ caused by the piezoelectric effect, the in-plane carrier density $\varrho$ per period and the energy of the electron $E_0$ at the bottom of the well. We integrate Eq. (1) using Eq. (2) and expand the root at the intermediate density regime $\varrho = \varrho_0/2 + \delta\varrho$,

$$T \propto \exp\left((\delta\varrho - \varrho_0)\underbrace{\sqrt{\frac{m_e e L_z^3}{36\hbar^2\epsilon_0\epsilon\varrho_0}}}_{=:\alpha} + O(\delta\varrho^2)\right). \qquad (3)$$

Since the carrier recombination is proportional to the square of the transmission coefficient $T$, we get

$$\frac{\partial_t\varrho}{\varrho} = -C_r|T|^2 = -C_r\exp\left[2\alpha(\delta\varrho - \varrho_0)\right], \qquad (4)$$

with the constant $C_r$ describing the optical transition probability. Neglecting the relative change in $\varrho(t)$ with respect to the change in $|T|^2$, we can approximate $\partial_t \ln(\varrho) \approx \frac{\partial_t\varrho}{\varrho_0/2}$ in the considered density regime. This is reasonable because $|T|^2$ changes by one order of magnitude while $\varrho$ only changes by a factor of 2, as is evident from the time dynamics of the luminescence (Fig. 4) and the calculations in Sec. V, Fig. 9. This approximation leads to an overestimation of the slope. Integrating from $[t_0, \varrho(t_0)]$ to $[t, \varrho(t)]$ gives

$$\delta\varrho(t) = \varrho_0 - \frac{1}{2\alpha}\ln\left(\alpha\varrho_0 C_r(t-t_0) + \exp\{2\alpha[\varrho_0 - \delta\varrho(t_0)]\}\right). \qquad (5)$$

We know from Eq. (2) that the transition energy changes with the carrier density $\varrho$ like $[E(\varrho) - E(0)] = \varrho\frac{eL_z}{4\epsilon\epsilon_0}$ corresponding to the screening of the band tilt. For times larger than the initial carrier decay time we can neglect the constant term in the logarithm, resulting in a logarithmic time evolution:

$$E(t) = \text{const} - \sqrt{\frac{9\hbar^2 e\varrho_0}{16\epsilon\epsilon_0 L_z m_e}}\ln(t - t_0). \qquad (6)$$

The slope is determined by the SL period $L_z$, the piezoelectric displacement charge $\varrho_0$ given by the strain and the piezoelectric coefficients, the effective electron mass $m_e$, and the dielectric constant $\epsilon$. If we calculate this

slope for sample II, we get a value of 67 meV, which is about two times larger than the experimental value given later in Fig. 5. This overestimation is attributed to the two main approximations made along the calculation and the use of the tunneling formula Eq. (1), which is only valid for situations where the change in the penetration depth is neglegible compared to the penetration depth itself, which is questionable at the beginning of the barrier. We, therefore, only get a qualitative expression for the slope, which is nevertheless helpful to understand the reason for the logarithmic time behavior and its dependence on the structural parameters. The behavior presented by Eq. (6) should be a general property of any superlattice with its band alignment governed by the internal piezoelectric fields as in the CdSe/CdS system.

## V. NUMERICAL MODEL

To get more quantitative results explaining the excitation dynamics of the considered superlattice, we apply a numerical model for the electronic states and the recombination processes. The density dependence of the subband transitions is determined by a self-consistent calculation of the energy levels and wave functions of the occupied subbands including the many-body effects charge-carrier screening and band-gap renormalization. The following assumptions are made to simplify the computation of the subband transitions: (1) effective mass approximation; (2) excitonic effects are neglected, e.g., we assume to be beyond the Mott density; (3) only the $A$ valence band of the hexagonal materials is considered. The $B$ valence band is separated in addition to the crystal-field split-off energy by a higher quantization energy due to the smaller effective mass and the $C$ valence band is separated even more by the spin-orbit split-off energy. Both are not occupied in the considered density regime. (4) Band-gap renormalization is included using the formula of Vashista and Kalia[18] for the local renormalization with the local bulk carrier density in the band as calculated from the subband wave functions and occupation. The results for the band-gap renormalization in this treatment are found to be in good agreement with published experimental data for GaAs quantum wells.[19,20] Since the band-gap renormalization is smaller than the charge-carrier screening in our case, this treatment should be sufficient. (5) Subband energies are calculated only for the discrete miniband dispersion points $k_z = 0$ and $\frac{\pi}{L_z}$. The subbands for a given band structure are calculated by a numerical diagonalization of the effective mass type Hamiltonian,

$$\mathcal{H} = V(z) + V_{\mathrm{cor}}(z) + \partial_z \frac{\hbar^2}{2m_{\mathrm{eff}}(z)} \partial_z . \tag{7}$$

Here $V(z)$ is the band-gap potential including the piezoelectric modifications and $V_{\mathrm{cor}}(z)$ is a correction potential consisting of the many-body effects charge-carrier screening and band-gap renormalization. As wave function basis for the numerical solution, we use a Fourier-series with the spatial frequencies $k/\frac{2\pi}{L_z} = 0, 1, \ldots, 2^n$ with $n = 5 \ldots 9$. The piezoelectric fields are calculated for a free-standing superlattice as described in Refs. 13 and 17. The given total carrier density is distributed among the subbands respecting Fermi-Dirac-statistics with given temperature. The total charge density $\rho(z)$ is determined using the subband carrier densities $\varrho_i^e, \varrho_i^h$ and their wave functions $\Psi_i^e, \Psi_i^h$:

$$\rho(z) = \sum_j e \left|\Psi_j^h(z)\right|^2 \varrho_j^h - \sum_i e \left|\Psi_i^e(z)\right|^2 \varrho_i^e . \tag{8}$$

The corresponding charge-carrier screening $V_{\mathrm{cor}}^{\mathrm{ccs}}$ is determined using Poison's equation and the boundary conditions $\int_0^{L_z} V_{\mathrm{cor}}^{\mathrm{ccs}}(z) dz = 0$ and $V_{\mathrm{cor}}^{\mathrm{ccs}}(0) = V_{\mathrm{cor}}^{\mathrm{ccs}}(L_z)$. The first one just fixes the absolute potential, the second one reflects the periodic boundary condition of the superlattice, which is established by surface charges creating spatially constant Fermi levels for electrons and holes. The band-gap renormalization $V_{\mathrm{cor}}^{\mathrm{bgr}}(z)$ of each band is calculated as decriped above. With this many-body correction $V_{\mathrm{cor}} = V_{\mathrm{cor}}^{\mathrm{bgr}} + V_{\mathrm{cor}}^{\mathrm{ccs}}$, we recycle the calculation for the conduction and valence bands until convergence.

In all our calculations we consider the carrier temperature as fixed at 50 K, but its absolute value is of minor importance for the results due to the big subband splitting in comparison to the thermal energy. The material parameters used in the calculation are listed in Table I.

This model is capable to calculate the electronic states in the SL as a function of the structural parameters and as a function of carrier density. In Fig. 5, the band structure and subband wave functions of an unexcited symmetric SL of 10 nm period length are plotted. One can realize the separation of electrons and holes and the tilted band structure due to the piezoelectric fields. We now give an oversight over the dependence of the electronic states on the structural parameters of the SL, namely, the period length and the ratio between the CdSe and the CdS layer thicknesses. The period-length dependence of the transition energies and the wave function overlap integrals of an unexcited symmetric SL is depicted in Fig. 5 for the transitions between the first

TABLE I. The material parameters of CdSe and CdS used in the calculations. See Ref. 21.

| | Parameter | CdSe | CdS | Unit |
|---|---|---|---|---|
| $E_G$ | band gap | 2.582 | 1.841 | eV |
| $m_{\parallel \vec{c}}^{\mathrm{CB}}$ | effective mass | 0.12 | 0.21 | $m_0$ |
| $m_{\parallel \vec{c}}^{A}$ | effective mass | 1.2 | 2.8 | $m_0$ |
| $m_{\nparallel \vec{c}}^{A}$ | effective mass | 0.45 | 0.68 | $m_0$ |
| $\epsilon_{\parallel}$ | dielectric constant | 9.91 | 9.12 | |
| a | lattice constant | 4.3 | 4.137 | Å |
| $C_1$ | | -0.76 | -1.36 | eV |
| $C_2$ | deformation | -3.7 | -2.28 | eV |
| $C_3$ | potentials | -4.0 | -1.54 | eV |
| $C_4$ | | 2.2 | 2.34 | eV |
| $c_{13}$ | elastic | 3.926 | 4.825 | $10^{10}$ N m$^2$ |
| $c_{33}$ | moduli | 8.451 | 9.575 | $10^{10}$ N m$^2$ |
| $e_{13}$ | piezocoefficients | -0.160 | -0.262 | C/m$^2$ |
| $e_{33}$ | | 0.347 | 0.385 | C/m$^2$ |

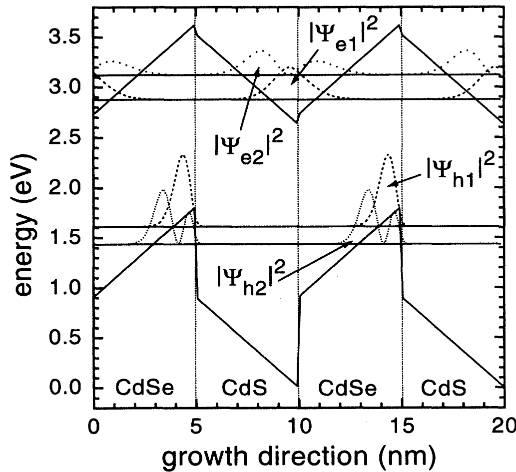


FIG. 5. Band structure and subband wave functions of a fully strained symmetric CdSe/CdS SL, with a period length of 10 nm for negligible carrier density.

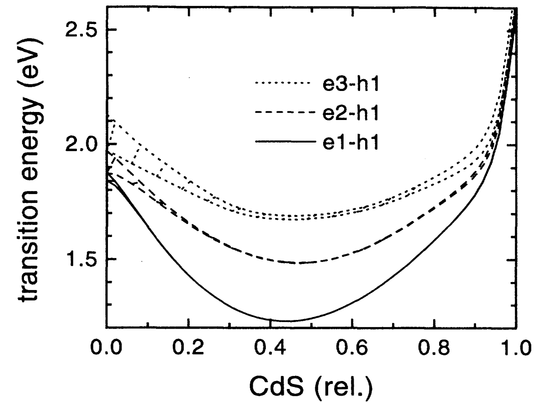


FIG. 7. Transition energies of a fully strained CdSe/CdS SL with 10 nm period length as a function of the relative CdS content. The transitions from the first three electron subbands to the first hole subband are plotted including the miniband splitting by the hatched areas.

three conduction-band states to the first hole state. We have selected these transitions because the higher conduction subbands get occupied at smaller densities than the higher valence subbands due to the different effective masses. One can realize the linear decrease of the transition energies with period length at larger periods reflecting the effect of the piezoelectric fields and an additional splitting of the minibands at small periods with a superlinear behavior corresponding to quantization effects. The $e1$-$h1$ overlap integral decreases dramatically

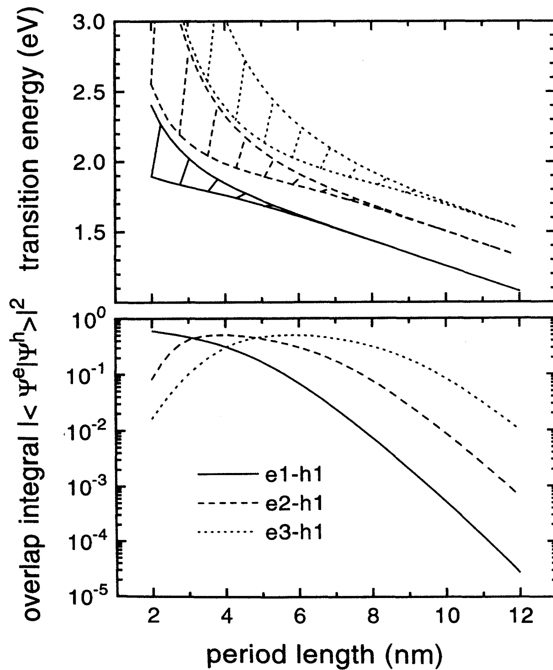


FIG. 6. Transition energies and overlap integrals of a fully strained symmetric CdSe/CdS SL as a function of period length. The transitions from the first three electron subbands to the first hole subband are plotted including the miniband splitting by the hatched areas.

with period length due to the spatial separation of the carriers. Additionally, the higher electronic states, which are forbidden transitions for very small period lengths, acquire higher overlap integrals for increasing $L_z$. This effect is important for the high excitation luminescence discussed in Sec. III. The influence of the ratio between the layer thicknesses of CdSe and CdS on the transition energies is depicted in Fig. 7, showing a minimum approximately at the symmetric case. This finding is due to the constant electronic chemical potential along the SL, equalizing the asymmetric part of the piezoelectric fields by an additional surface charge density. The subband width increases with the asymmetricity of the SL due to the narrowing of the barrier for the electrons.

As one excites carriers into the SL, the carriers get separated into adjacent layers leading to an electrostatic field that tends to screen the piezoelectric fields. This charge-carrier screening is visualized in Fig. 8, where we have depicted the band alignment of a symmetric SL with 10 nm period length at an excitation density of $2 \times 10^{13}$ electron-hole pairs per $cm^2$ and period (compare with Fig. 5). One can realize the bending of the bands due to the many-body effects charge-carrier screening and band-gap renormalization, which are separately depicted in the lower part of the figure. The charge-carrier screening is dominant over the band-gap renormalization in this case due to the long period length. We have calculated the resulting density dependence of the lowest transition energy for symmetric SL's of different period lengths (Fig. 9) to display the counterplay between charge-carrier screening and band-gap renormalization. The qualitative behavior of the density dependence reveals a significant change with period length. For small lengths, the band-gap renormalization results in an effective redshift of the transition with density, whereas the charge-carrier screening is small due to the minor seperation of the carriers. With increasing period, the charge-carrier screening becomes dominating and an initial redshift due to band-gap renormalization turns to a blueshift with density by the charge-carrier screen-

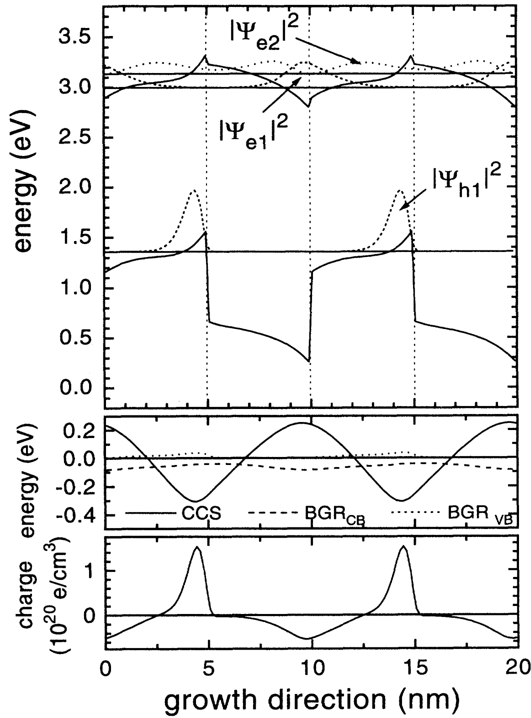


FIG. 8. Band structure, subband wave functions, charge density, electrostatic potential, and band-gap renormalization in a fully strained symmetric CdSe/CdS SL with 10 nm period length at a carrier density of $2 \times 10^{13}/\mathrm{cm}^2$ per SL period (compare with Fig. 5).

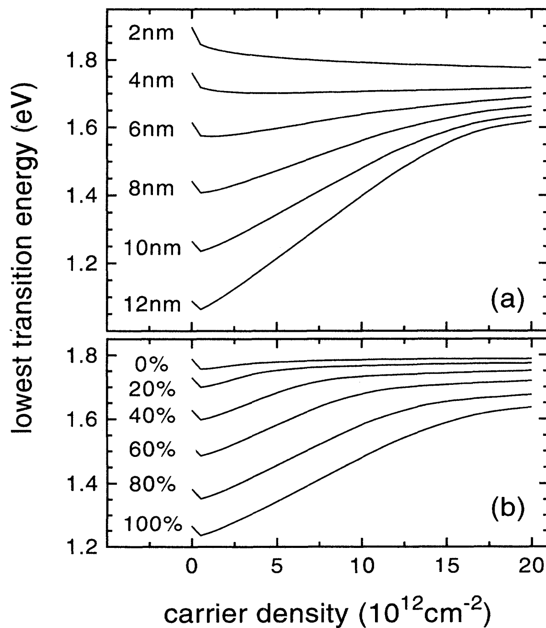


FIG. 9. The lowest transition energy of a symmetric CdSe/CdS SL as a function of the carrier density (a) fully strained for several period lengths (b) with a period length of 8 nm for various relative strains.

ing. This reflects the different density dependence of the charge-carrier screening, showing a linear variation with the density $n$, compared to the band-gap renormalization, which varies approximately like[20] $n^{1/3}$.

The linear blueshift with density then continues up to a saturation density of about $1.5 \times 10^{13}/\mathrm{cm}^2$ per period. Starting from this density, the screening of the piezoelectric fields leads to a significant spreading of the wave functions, which reduces the separation of the carriers (see Fig. 8) and thus reduces the charge-carrier screening. This saturation density is given by the displacement charge density at the interfaces caused by the piezoelectric effect, which equals $1.87 \times 10^{13} e/\mathrm{cm}^2$.

At longer period lengths, the strain relaxes partly by the creation of dislocations.[7] We have addressed this behavior by taking into account different strain relaxation coefficients, assuming the strain to be homogeneous along the SL [Fig. 9(b)], while the exact strain distribution is not known by now. The relaxation reduces the piezoelectric fields and consequently leads to an blueshift of the transition energies and a reduction of the saturation density, as can be seen from the bending of the density dependent curves.

The density dependence of the overlap integrals of the $e1$-$h1$ and the $e2$-$h1$ transitions (Fig. 10) shows a strongly period length dependent behavior. At a period length of 2 nm, the density only weakly influences the overlap integrals, due to the small carrier seperation. With increasing period length, the piezoelectric fields and the charge-carrier screening gets more important for the band structure, resulting in a strong density dependence of the overlap integrals of up to two orders of magnitude. This fact determines the carrier recombination dynamics in these SL's.

To compare these numerical results with the time-resolved experiment, the dynamics of the carrier-recombination is calculated by a determination of the instant carrier decay time $\tau(n)$ for a given density $n$ out of the average wave function overlap of the occupied sub-

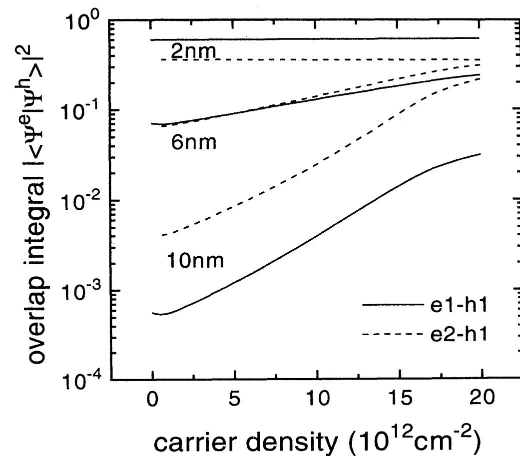


FIG. 10. Overlap integrals for the transition from the first and the second electron subband to the first hole subband in a fully strained, symmetric CdSe/CdS SL as a function of carrier density for several period lengths as indicated.

band states multiplied with a constant band-band transition matrix element. The latter value is assumed to be constant with density. This results in

$$n\tau(n,T) \propto \sum_{i}^{e}\sum_{j}^{h} |\langle \Psi_i^e|\Psi_j^h\rangle|^2 \times \int_0^\infty f_{\rm FD}(E_i^e + E_{\rm kin}^e, \mu_e, T) \times f_{\rm FD}(E_j^h + E_{\rm kin}^h, \mu_h, T) dE_{\rm kin} \quad (9)$$

with the Fermi Dirac distribution $f_{\rm FD}$, the Fermi energies $\mu_{e,h}$, the subband wave functions $\Psi_i^e$, $\Psi_j^h$, and the kinetic energies of electrons and holes given by the momentum conservation $E_{\rm kin}^{e,h} = m_{h,e}/(m_e + m_h)E_{\rm kin}$. Integration of the carrier decay from the starting values ($n = n_0$,$t = 0$) leads to the time dependence of the density, given implicitly by $t(n)$,

$$t(n) = \int_n^{n_0} \frac{\tau(n,T)}{n'} dn' \ . \quad (10)$$

We depict in Fig. 11 the temporal evolution of the lowest transition energy for different period lengths of a symmetric SL for a constant bulk initial carrier density of $2 \times 10^{19}/{\rm cm}^3$ coming along with equal excitation intensities. Short period SL's exhibit a blueshift, while longer period SL's show a redshift of the transition energy with time. This property reflects the density dependent behavior of the transition energy as dicussed previously. It is remarkable that, for period lengths above 8 nm, the transition energies show very similar time evolutions with a nearly logarithmic part at intermediate times. This leads to nearly equal onsets of the luminescence dynamics for SL's with period lengths above 8 nm. These predictions are confirmed by the experimental observation shown in Fig. 9. The samples II and III with the larger period lengths of 8 nm and 12 nm reveal a similar logarithmic behavior, whereas the results for sample I with the shortest period are blueshifted due to the higher quantization energy (see Fig. 6) and reveal only a blueshift due to the band-filling, compensating the band-gap renormalization of the subband gap.

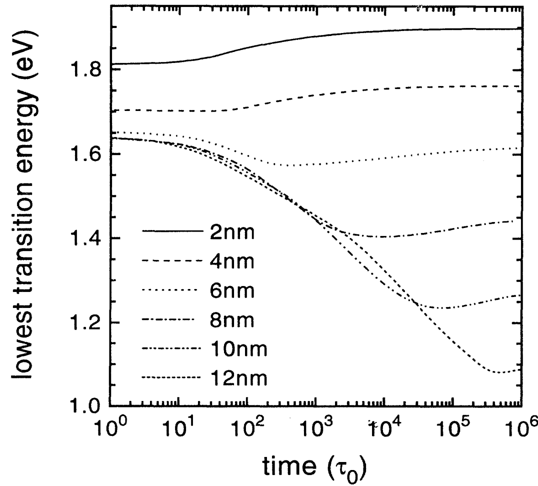


FIG. 11. Calculated time development of the lowest transition energy of fully strained symmetric CdSe/CdS SL's for an initial density of $2 \times 10^{19}/{\rm cm}^3$ . The different period lengths are indicated at the corresponding curves. The time unit $\tau_0$ is the bulk band-band lifetime.

## VI. NONLINEAR ABSORPTION

The absorption and nonlinear absorption gives information about all optically active subband transitions. In Fig. 12 the results for sample III with removed substrate are given. The absorption (a) consists of three parts. In the low energy part up to about 1.8 eV the sample is transparent and reveals pronounced Fabry-Pérot modes induced by the high refractive index of the layer. At higher energies the SL absorption sets in smoothly and

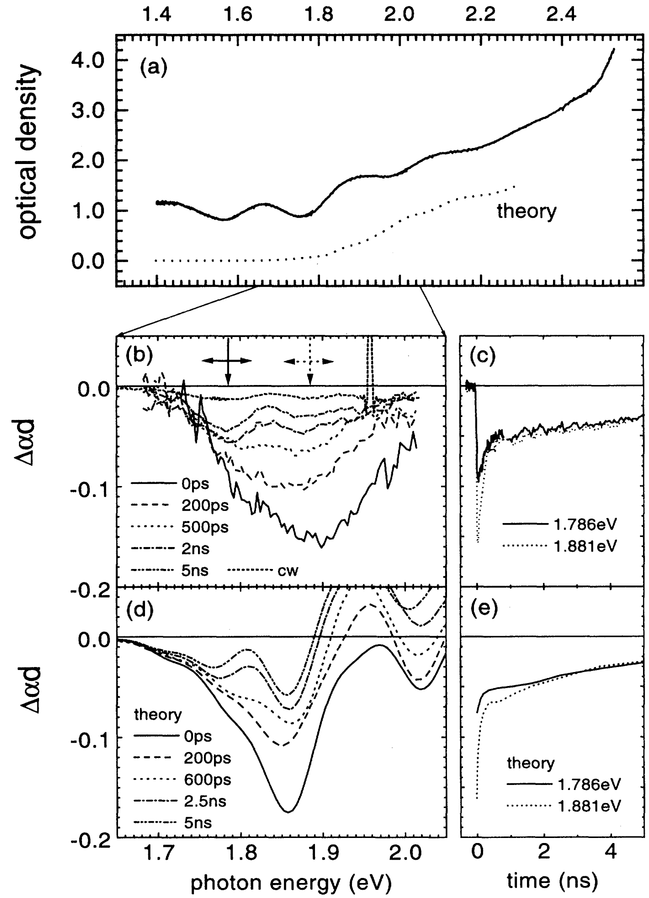


FIG. 12. (a) Absorption of the CdSe/CdS SL sample III at a lattice temperature of 20 K under low excitation. Experimental (solid line) and theoretical (dotted line) result are plotted. (b) and (c) Time development of the nonlinear absorption after excitation with 70 ps pulses at 2.46 eV with $0.46\,{\rm mJ/cm}^2$. (b) Spectrally resolved at several delay times after excitation. The curve marked with cw is the nonlinear absorption under continuous excitation of $0.5\,{\rm W/cm}^2$ with an He-Ne laser. (c) Temporally resolved at the two energetic positions indicated with arrows in (b). (d) and (e) Theoretical results corresponding to (b) and (c). The initial density is $9 \times 10^{12}/{\rm cm}^2$ per period.

beginning from 2.5 eV the CdS buffer and cladding layer band-edge gives rise to a steep absorption edge. The theoretical absorption of the SL, as calculated from the band structure, agrees with the experimental data (dotted line).

The nonlinear absorption [(b) and (c)] shows a bleaching of the SL absorption, which consists of two components as indicated by arrows and reveals a fast and a slow component. The fast one during the first 500 ps is a consequence of the clearing of the occupation in the higher electronic states, which is fast due to the large overlap integrals of these transitions (see Figs. 6 and 10). Once these higher electron subbands are emptied, the carriers recombine only from the $e1$ to the $h1$ state with a longer and density dependent lifetime, due to the small and density dependent overlap integrals (Fig. 10). This is the reason for the slow component in the nonlinear absorption, which is caused by the occupation of the $h1$ subband. This component is also observable under continuous excitation with a He-Ne laser [see Fig. 12(b)]. The bleaching of the ($e1$-$h1$) transition is not observable in this experiment due to its comparatively weak oscillator strength (see Fig. 6). These results are compared with the theoretical results depicted in (d) and (e) as calculated using the numerical model presented in Sec. V. They are in good agreement with the experimental results. We can assign the two components in the experimental spectra mainly to the bleaching of the ($e2$-$h1$) and ($e3$-$h1$) transition, respectively. There are additional contributions by the shift of the transition energies due to band-gap renormalization and charge-carrier screening which add to the nonlinear signal and thus complicate the picture. The deviation in (d) compared to (c) is attributed to the overestimation of the band-gap renormalization of higher subbands by the local density treatment, leading to the induced absorption in the theoretical results.

## VII. CONCLUSION

We have demonstrated that the many-body effects charge-carrier screening and band-gap renormalization give rise to a pronounced nonlinear behavior in the CdSe/CdS Stark SL system. We have presented a qualitative analytical and a quantitative numerical model, which gives a detailed understanding of the processes involved in the many-body properties of this SL system.

## ACKNOWLEDGMENTS

This work has been supported by the "Deutsche Forschungsgemeinschaft" and the "Materialschwerpunkt der Universität Kaiserslautern." Stimulating discussions with Dr. H. Kalt and Dr. M. Grün are gratefully acknowledged.

[1] D.L. Smith and C. Mailhiot, Phys. Rev. Lett. **58**, 1264 (1987).
[2] X. Zhang, K. Karaki, H. Yaguchi, K. Onabe, R. Ito, and Y. Shiraki, Appl. Phys. Lett. **64**, 1555 (1994).
[3] B.K. Laurich, K. Elcess, C.G. Fonstad, J.G. Beery, C. Mailhiot, and D.L. Smith, Phys. Rev. Lett. **62**, 649 (1989).
[4] K.J. Moore, P. Boring, B. Gill, and K. Woodbridge, Phys. Rev. B **48**, 18 010 (1993).
[5] T.S. Moise, L.J. Guido, R.C. Barker, J.O. White, and A.R. Kost, Appl. Phys. Lett. **60**, 2637 (1992).
[6] R. André, C. Deshayes, J. Cibert, Le Si Dang, S. Tatarenko, and K. Saminadayar, Phys. Rev. B **42**, 11 392 (1990).
[7] M. Grün, M. Hetterich, C. Klingshirn, A. Rosenauer, J. Zweck, and W. Gebhardt, J. Cryst. Growth **138**, 150 (1994).
[8] W. Langbein, H. Kalt, M. Hetterich, M. Grün, and C. Klingshirn, Appl. Phys. Lett. **65**, 2466 (1994).
[9] W. Langbein, H. Kalt, M. Hetterich, M. Grün, and C. Klingshirn, J. Cryst. Growth **138**, 191 (1994).
[10] M.P. Halsall, J.E. Nicholls, J.J. Davies, P.J. Wright, and B. Cockayne, Surf. Sci. **228**, 41 (1990).
[11] M. Grün, C. Klingshirn, A. Rosenauer, J. Zweck, and W. Gebhardt, Appl. Phys. Lett. **63**, 2947 (1993).
[12] M. Hetterich (private communication).
[13] M.P. Halsall, J.E. Nicholls, J.J. Davies, B. Cockayne, and P.J. Wright, J. Appl. Phys. **71**, 907 (1992).
[14] D. Wolverson, M.P. Halsall, and J.J. Davies, Semicond. Sci. Technol. **6**, A123 (1991).
[15] X. Chen, P.J. Parbrook, C. Trager-Cowan, B. Henedrson, K.P. O'Donnel, M.P. Halsall, J.J. Davies, J.E. Nicholls, P.J. Wrigth, and B. Cockayne, Semicond. Sci. Technol. **5**, 997 (1990).
[16] M. Grün, W. Langbein, H. Hetterich, and C. Klingshirn, Superlatt. Microstruct. (to be published).
[17] E. Anastassakis, Phys. Rev. B **46**, 4744 (1992).
[18] P. Vashista and R.K. Kalia, Phys. Rev. B **25**, 6492 (1982).
[19] J.C. Ryan and T.L. Reinecke, Phys. Rev. B. **47**, 9615 (1993).
[20] G. Tränkle, H. Leier, A. Forchel, H. Haug, C. Ell, and G. Weimann, Phys. Rev. Lett. **58**, 419 (1987).
[21] *Semiconductors*, edited by O. Madelung, Landolt-Börnstein, New Series, Group III, Vol. 17 (Springer, Berlin, 1982), pp. 166–224; *ibid.*, Vol. 22 (Springer, Berlin, 1986), pp. 194–216.